Effects of Blood Pressure and Intraocular Pressure on Ocular Arterial Blood Flow: Studies on *in vitro* Models

Honors Research Thesis

Presented in Partial Fulfillment of the Requirements for Graduation with *research distinction* in Biomedical Engineering in the Undergraduate Colleges of The Ohio State University

By

Sunny Kwok

The Ohio State University

April 2018

Project Advisor: Dr. Jun Liu

Department of Biomedical Engineering

Abstract

Glaucoma is the second leading cause of blindness around the world. Diagnosis of this disease often occurs after the detection of noticeable symptoms, by which point irreversible damage has already been incurred. Glaucoma develops when stress factors induce retinal ganglion cell death, resulting in vision loss. In particular, prolonged reduction in blood flow into the eye may lead to ocular tissue malnutrition and hypoxia, eventually leading to cell death. The posterior ciliary arteries are the main blood supply to the optic nerve head, where glaucoma damages occur first. These arteries traverse the posterior peripapillary sclera to penetrate the eye. This study aims to investigate the effects that different combinations of intraocular pressure, blood pressure, and scleral stiffness have on blood flow of *in vitro* posterior ciliary artery models. To perform this study, a modeling system of the peripapillary sclera was developed. A number of different polymers (including agarose, polydimethylsiloxane, and industrial TC-5005 gels) were explored to model scleral tissues with various compressive moduli. Multiple models of industrial TC-5005 and agarose were made to mimic sclera of increasing stiffness. The polymers were molded and cured into wall-less vessels and placed into a perfusion chamber where pressure was separately applied to the outside (intraocular) and inside (blood) the vessel at different combinations. Five models of stiffness ranging from 30 – 415 kPa were fabricated for flow tests. The resulting change in fluid flow rate was recorded to determine the combinatory effects of the two pressures through these phantoms. It was found that across all combinations of pressures, the fluid flow would initially increase with stiffness, then upon reaching ~60 kPa achieve a maximum flow. For models much stiffer than 60 kPa, a significant decrease in fluid flow as much as 87% was observed. The initial increase in fluid flow from 30 to 60 kPa may be evidence of the protective effects of scleral stiffening predicted in previous research. This study represents a first step in understanding the

potential impacts of the scleral compressive modulus on the fluid flow rate under biological effects by IOP and BP, supporting the hypothesis that sclera stiffness may play an important role in glaucomatous development.

Acknowledgement

The author acknowledges Dr. Jun Liu for her guidance as the primary advisor to this project as well as for serving on the defense committee. The author would like to acknowledge Keyton Clayson, Yanhui Ma, Eli Pavlatos, and Thomas Sandwisch for helpful discussions and advice. Dr. Lakshmi Dasi is acknowledged for helpful discussions and serving on the defense board. Dr. Cynthia Roberts and her students Boihan Audrey Nguyen and Monica Okon must also be acknowledged for their insights and guidance. The author would also like to thank Hanyang Huang and Lin Qi from Dr. Yi Zhao's lab for guidance with polymer material selection as well as Pengfei Jiang and Dr. Katelyn Swindle-Reilly for further clarification on polymer fabrication and material science knowledge.

Table of Contents

List of Figures

List of Tables

I. Introduction

Glaucoma is often simply viewed as a disease in which an increased level of pressure within the eyeball eventually results in blindness. In the past, diagnosis of glaucoma was heavily reliant on the presence of high intraocular pressure (IOP). The leading theory was that a chronically elevated IOP level would continuously apply stress to the optic disc, eventually leading to deterioration of the ganglion cell layer in the eye (He, Vingrys, Armitage, & Bui, 2011; Jia, Yu, Liao, & Duan, 2016; Ramanathan & Ernest, 1998). Hamzah & Azuara-Blanco reported that as much as 50% ganglion cell death can occur before any noticeable symptoms may be detected, but by that point irreversible damage has already been done.

In fact, glaucoma affects more than 66 million people worldwide; however, the true causes of this debilitating disease are still under much scrutiny (Hamzah & Azuara-Blanco, 2010). While high IOP levels may increase the risk of developing glaucoma, there are many cases in which patients diagnosed with glaucoma do not show any abnormalities in IOP levels. There have also been cases in which people with high IOP levels do not end up developing glaucoma. Numerous studies have been done to investigate other potential factors that may contribute to the development of glaucoma. Research has been done exploring the effects of age-related deteriorations, ethnic predispositions, family glaucomatous history, central corneal thinning, and others in a plethora of large-scale studies (He et al., 2011). Regardless of cause, there is consensus in the field that glaucomatous pathogenesis can be attributable to damage of retinal ganglion cells.

Relevant Ocular Anatomy and Physiology

The human eye receives light through the cornea which focuses the light through the lens to reach the retina at the back. The retina consists of hundreds of thousands of ganglion nerve cells

that convert the light image into electrical impulses that is carried to the brain by the optic nerve. The optic nerve enters the posterior of the eye by penetrating the peri-papillary scleral layer and through the fenestration of the lamina cribrosa, this segment of the nerve being termed the optic nerve head (ONH). The ophthalmic artery trifurcate into the central retinal artery (CRA), the long posterior ciliary artery (lPCA), and the short posterior ciliary artery (sPCA). Along with the optic nerve, the sPCA also penetrate the sclera in order to feed the choroid and retina while the CRA enters the eye in between the optic nerve (Fig. 1). The ONH itself also obtains its oxygen and nutrients primarily from branches of the sPCA (Prada et al., 2016; Yanoff & Sassani, 1994). Maintaining a constant blood flow to this region is critical in supporting the functions of the eye.

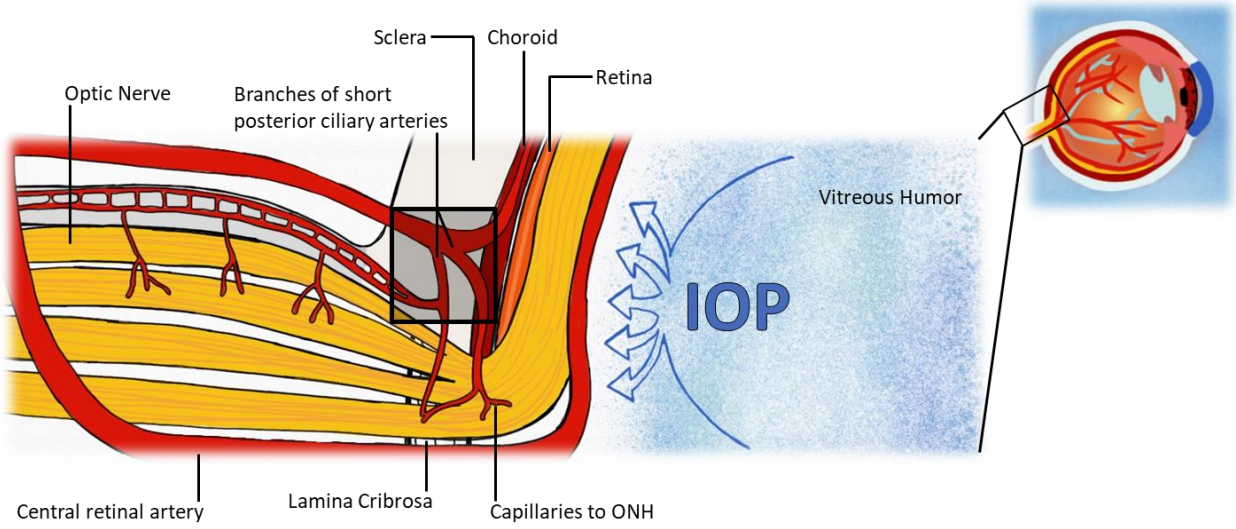

Figure 1. Schematic of ONH; shaded rectangle denotes the area of interest

Like many other vasculatures to important organs of the body, the vessels to the eye exhibit the ability to engage autoregulation in order to maintain a relatively constant blood flow (Pillunat et al. 1997, Riva, Cranstoun, & Petrig, 1996). The vascular smooth muscles of the blood vessels are capable of vasoconstriction and vasodilation in response to the fluctuations in arterial pressure. Changing the vessel diameter in turn changes the vessel's resistance to flow. However,

autoregulation has a limited range of effect, outside of which the blood flow derails from optimal range. Pillunat et al. found that in humans, IOP greater than 45 mmHg resulted in declines in blood flow. While this may not cause immediate damage in the short run, prolonged reduction in blood flow may contribute to retinal ganglion cell death. The mechanisms of ocular autoregulation are still not well understood. For example, there has been evidence that the efficiency of the autoregulation within the choroid varies given different stressors (Schmidl, Garhofer, & Schmetterer, 2011). This phenomenon may in fact be due to the contributions of neural mechanisms at work and remains to be studied.

Pressure and Fluid Flow

Recently, more interest has been focused on the effects of blood pressure (BP) on the blood flow through the ONH. The heart continuously pumps oxygenated and nutrient-rich blood through the body's vasculature. The pumping of the heart produces the driving force of blood flow, the blood pressure. The mean arterial BP constantly varies between the systolic and diastolic limits that correlate to the contraction and relaxation of the heart, respectively. For the average human, this value is around 120/80 measured from the brachial artery. As the vasculature branches off, the BP and blood flow is reduced as the vessels diminish in size to allow for the diffusion of oxygen and nutrients to occur in the capillaries. The mean arterial pressure in the ophthalmic artery, for example, is about 90/70 (Hayreh & Edwards, 1989). Further branching from a main artery has been characterized through experimentation; specifically, it's been shown that by the time blood reaches capillary vessels, the pressure drops to as low as 20 mmHg to allow for optimum oxygen and nutrient diffusion (Lombard, 1912). It can be assumed that the branches of the ophthalmic

artery, PCAs and CRA, would experience a reduction in blood pressure down to the level of capillaries as they continue to divide.

Since the sPCA penetrates the scleral layer, that segment of the artery is also under the mechanical effects from IOP. IOP is the fluid pressure exerted by production and drainage of the aqueous humor. The normal human IOP range of 10 – 20 mmHg is necessary for the eye to maintain its shape. As IOP pushes outward against the structures of the globe, the scleral layer becomes compressed. So while the sPCA travels through the sclera, its branches also experiences a slight compressive force, potentially resulting in a decrease in fluid flow. With high enough IOP compressing the vessels, a substantial reduction in blood flow may occur resulting in ischemic microenvironments. Furthermore, IOP has been found to significantly correlate to changes in BP, increasing by as much as 0.4 mmHg for every 10 mmHg increase in BP (Klein, Klein, & Knudtson, 2005). This may be another possible mechanism of autoregulation to maintain ocular blood flow.

In studying the relationship between blood pressure and intraocular pressure, it is critical to observe the ocular perfusion pressure (OPP), which differs from the typical calculation as the difference between arterial and venous pressure. OPP refers to the perfusion pressure that drives blood flow within the intraocular vessels (Prada et al., 2016):

$$\text{OPP} = \frac{2}{3}\,\text{MAP} - \text{IOP}$$

where

$$\text{Mean Arterial Pressure (MAP)} = \text{diastolic BP} + \frac{1}{3}\,(\text{systolic BP} - \text{diastolic BP})$$

Without the effects of autoregulation, a decrease in OPP, that is to say a decrease in BP or an increase in IOP, reduces the blood flow. This causes a reduction in oxygenation and nutrition of the cells eventually leading to regional cell apoptosis (Cherecheanu et al., 2013). This relationship between the OPP, BP, and IOP can also explain why the current method of decreasing IOP levels is such a common treatment for patients diagnosed with glaucoma. On the other hand, He et al. in their comprehensive review found that 11 studies reported significant correlation between glaucoma and high BP, yet 10 other studies have reported links between glaucoma and low BP. Furthermore, it intuitively makes sense that low BP may lead to glaucoma as it would reduce OPP, thereby increasing the risk of retinal ganglion cell apoptosis. On the other hand, a higher OPP could result from hypertension, which would in fact induce a protective effect. Nevertheless, studies have also shown an increased risk of developing glaucoma in patients diagnosed with hypertension. This contradictory relationship between ocular perfusion pressure (resulting from a combination of BP and IOP) and the resultant risk of developing glaucoma requires further study.

Aside from perfusion pressure, fluid flow is also highly dependent on the physical fluid properties. For example, blood flow is determined by the non-Newtonian properties of blood. Importantly, for non-Newtonian fluids such as blood, the fluid viscosity is highly dependent on the shear rate against the blood vessel (Johnston, Johnston, Corney, & Kilpatrick, 2004). In many cases, blood flow may be simplified into a Newtonian flow model under steady-state laminar flow. Eduard Hagenbach and Jean Poiseuille derived the Hagenbach-Poiseuille's Law from the Navier-Stokes equation to characterize Newtonian flow (Skalak, 1993):

$$Q = \pi r^4 P / 8\mu L, \qquad R = 8\mu L / \pi r^4, \qquad P = Q*R$$

where

Q = fluid flow	r = tube radius
P = blood pressure	μ = viscosity
L = length	R = resistance

This law describes a direct relationship between pressure and flow rate that varies by the resistance coefficient, R. As pressure change increases, it can be expected that given the same tube structure, and therefore a constant resistance, flow rate will increase linearly. It is also important to note that the flow resistance is hugely affected by the tube radius (r^4), resulting in a drastic increase in resistance with only a small change in the vessel radius. This simplified relationship may provide insight for how fluid flow vary under changing IOP and BP.

Scleral Stiffness

The sclera makes up the structural casing of the eye, protecting the delicate mechanisms within. Due to IOP, the scleral layer is constantly inflated and under a compressive force. The sclera's stiffness, quantified by its compressive modulus, has been measured in a variety of ways. Average scleral stiffness has been found to be within the range of 5 to 60 kPa using a uniaxial compression system (Battaglioli & Kamm, 1984; Mortazavi, Simon, Stamer, & Vande Geest, 2009). Other methods have found scleral stiffness to be much higher, reaching as high as 300 kPa (Coudrillier et al., 2012). It has been hypothesized that soft, or "weak" sclera could also represent a risk factor for glaucomatous development. Eilaghi et al. developed a finite element model to discern the effects of stiffness on the resultant IOP-induced strain in ONH structures such as the lamina cribrosa. They found that their soft scleral model exhibited a much higher level of strain in

the ONH than previously reported data, even at normal levels of IOP (Eilaghi, Flanagan, Simmons, & Ethier, 2009).

Scleral stiffening has been under consideration as a potential protective measure that naturally occurs through aging to protect the lamina cribrosa from IOP-induced deformation. The lamina cribrosa maintains the pressure gradient between the IOP and the surrounding tissue by deforming posteriorly. However, it is thought that increased IOP would result in pinching of the laminar meshwork and mechanical damage to the ONH which traverses it (Prada et al., 2016, Quigley et al., 1981). It has been well documented that scleral stiffening occurs with aging (Fazio et al., 2014; Palko et al., 2016; Wensor, Stanislavsky, Livingston, & Taylor, 1998). Coudrillier et al. also found that peripapillary scleral stiffening is effective at reducing the magnitude of biomechanical strains within the lamina cribrosa (Coudrillier et al., 2016). Furthermore, stiffer sclera may restrict arterial vessel wall compliance and reduce IOP-effects, thereby allow for increased BP. Blood pressure increase would induce a higher OPP, effectively reducing the risk for glaucoma. Yet, there are also reports that increased stiffening of the scleral layer may result in intensifying the strain response in other softer tissues (Quigley & Cone, 2013). The exact effects of scleral stiffness in regards to nerve damage in the eye is still a mystery, and has only recently begun to attract research attention.

No clear link has been made of exactly how BP, IOP, scleral stiffness, and the blood flow rate relate to each other and ultimately, affect the development of glaucoma. With a stronger understanding of these factors and their relationships with each other, we may be able to find other avenues for diagnosing glaucoma. The complex mechanics, interactive anatomy, combined with the many possible risk factors make studying the diseases of the eye especially complicated; our research model simplify the complexities of the eye's anatomy first into the phantom model. Here,

we propose an *in vitro* model to study the effects of blood pressure and intraocular pressure on the ciliary arterial flow rate in polymer phantom models mimicking peri-papillary scleral tissue at various degrees of stiffness.

II. Methodology

Perfusion Chamber Design

To be able to collect perfusion data, a unique chamber was developed. The chamber main body is cut from a cylindrical tube of acrylic that is fitted into a square top and base plate with rubber O-rings to prevent leakage. The top and base pieces are tapped and threaded to further seal the device. Around the midsection of the chamber, four threaded holes were staggered in height to fit connectors for the following purposes: 1) BP pressure column, 2) IOP pressure sensor, 3) Outlet and BP pressure sensor, 4) IOP pressure column (Fig. 2). During the phantom curing process, a 21-gauge needle (800 ± 3 μm) was inserted through connectors 1 and 3 to form a wall-less vessel, mimicking a 3-cm segment of the posterior ciliary artery.

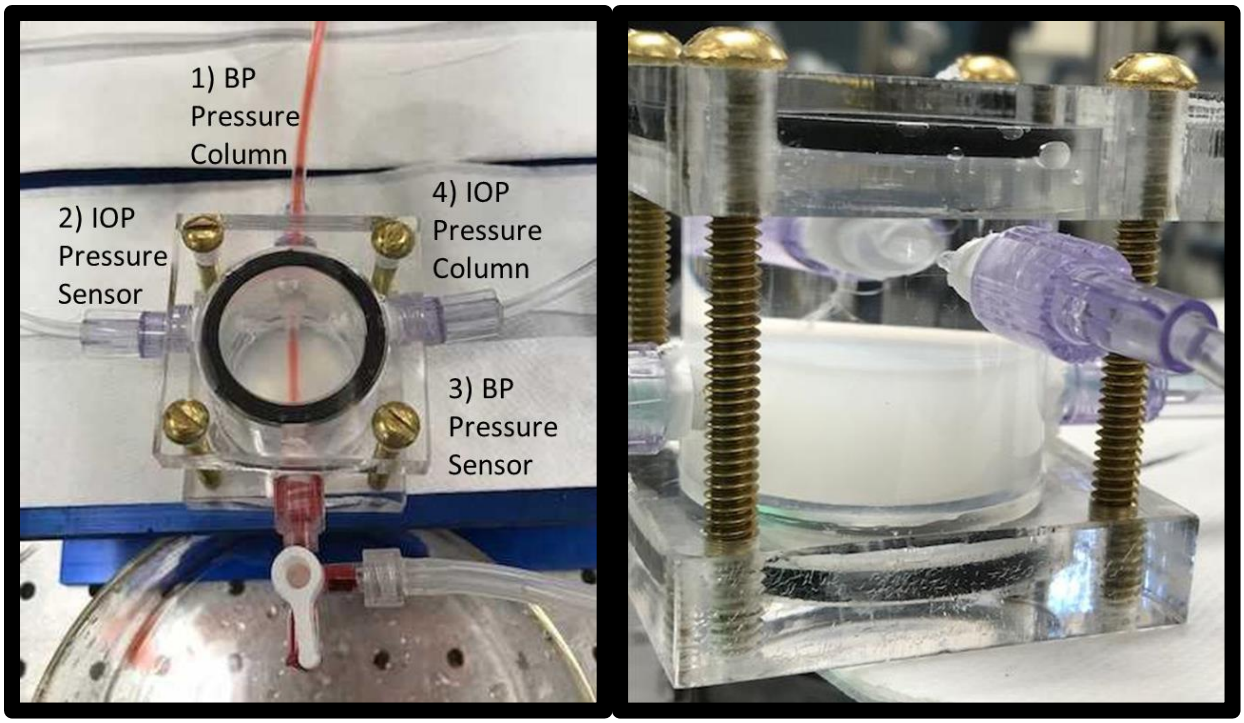

Figure 2. Perfusion Chamber Design; top view of the perfusion chamber and its attachments (left); side view of the perfusion chamber with TC-5005 phantom (right)

Polymer Phantom Fabrication

Multiple polymers were tested in an effort to produce phantoms with stiffness comparable to scleral tissue. The phantoms used here were made from either agarose (Low-EEO/Multi-Purpose/Molecular Biology Grade, Fisher BioReagents) or industrial TC-5005 (BJB Enterprises). Four models, two different agarose and two different TC-5005, were ultimately tested in the perfusion flow analysis.

Agarose phantoms were made by dissolving various weights (in grams) of the powder in distilled water volume (in mL) ranging from 0.6 – 0.9% and then mixed at 70°C for 15 minutes. 10 mL of the resultant mixture was poured into the perfusion chamber and left to cure for at least 8 hours. 1.5 mL of agarose was poured into a cell culture dish (60 mm × 15 mm) and left to cure

for at least 8 hours. Polymer disks (10 mm× 1.5 mm) were cut out with a 10 mm Trephine blade to use in mechanical compression tests.

Industrial TC-5005 phantoms were made by combining its three agents (A, B, and C) in various units. Per the factory instructions, increasing agent C would result in a more elastic polymer. Each phantom was made with a set A and B ratio (100 to 20 units) while increasing agent C from 40 to 50 units. 10 mL of the mixture was poured into the perfusion chamber, degassed for 30 minutes, and then allowed to cure at 27°C for at least 16 hours. 1.5 mL of TC-5005 was used to form compression disks.

Polydimethylsiloxane (Sylgard 184 PDMS, Dow Corning) polymers were also tested for its stiffness in comparison to sclera. PDMS disks were made by combining its two agents (A and B) in 100 to 12 units, respectively. The mixture was degassed for 30 minutes, then poured into a cell culture dish and cured in an oven at 60°C for 2 hours. PDMS was not ultimately used to make perfusion phantoms.

Compression Test Protocol

To measure the compressive properties of the polymer phantoms, mechanical compression tests were done using a modified Bose System (ElectroForce Planar Biaxial TestBench, Bose Corporation, Eden Prairie, MN, USA). The system consists of a mover plate controlled by the Bose speakers that provides displacements up to micron resolution and a load plate connected to the load cell that measures force in Newtons (Fig. 3). Fixtures for compression tests were made using 3D printing. The compression disk was placed on the load plate and gently moved manually to barely come into contact with the mover plate. The system then automatically adjusts to provide

a preload of 0.015 N of compressive force was applied to ensure that contact with the material was made.

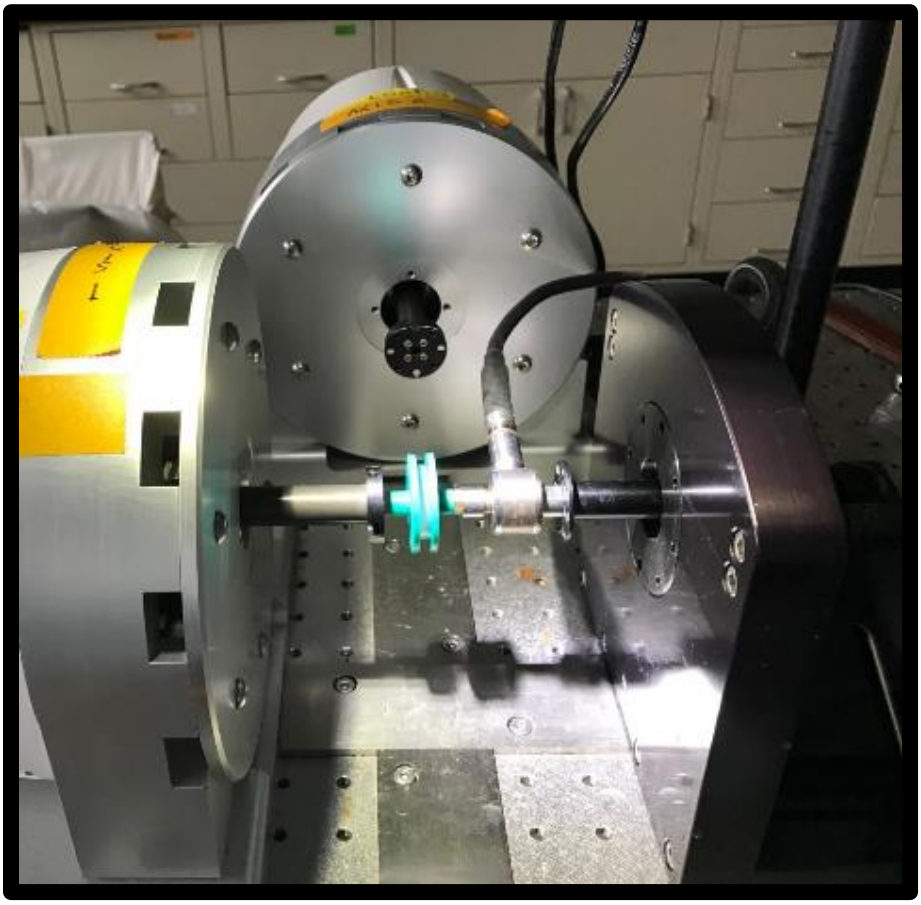

Figure 3. Compression test with agarose sample in the Bose System

For agarose disks, compression tests were run for 10% strain over 2 minutes. To maintain the hydration of the agarose, the agarose samples were kept submerged in distilled water before testing. Since TC-5005 and PDMS were both found to be stiffer than agarose, compression tests were only run for 2% strain to reduce stress to the load cell. The Bose system recorded both the displacement (mm) and the resultant force (N) for each test. Each dataset was fitted with a linear trend-line, the slope of the resultant curve is recorded as the compressive modulus, E. The compressive modulus was calculated using the following equation:

$$E = \sigma/\varepsilon$$

where

σ = Force/Area,

ε = Displacement/Original Length

Three disks were tested for each batch of polymers and the average compressive modulus was taken as the stiffness of its respective phantom model. For the four phantom models, a total of 12 compression tests were completed.

Flow Test Protocol

After curing each phantom, the space above the polymer was filled with distilled water. Connecting this chamber to a hydrostatic column through connector 4 allowed a simulation of IOP forces against the top face of the phantom. Connector 1 led to another hydrostatic column that applied a BP to the distilled water which flowed through the wall-less vessel. The distilled water was stained with food coloring to better visualize the fluid flow and distinguish it from the water in the IOP chamber. Connector 2 was attached to a pressure sensor for the IOP chamber. Connector 3 was connected to a three-way nozzle that had an outlet for the fluid flow and an outlet to measure the BP through the wall-less vessel. The complete setup can be seen in Figure 4.

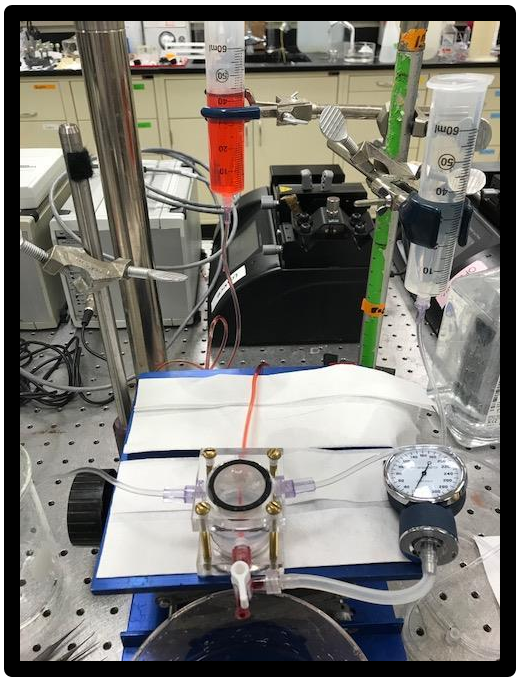

Figure 4. Complete setup for flow tests

Flow tests were performed for different combinations of BP and IOP. BP ranged from 20 – 40 mmHg and IOP ranged from 10 – 40 mmHg which can be adjusted by raising or lowering the hydrostatic columns. Pairing each pressure step, there were a total of 12 combination per phantom. For every interval, the system was allowed to rest for 1 minute. Then, the outlet was opened to allow fluid to flow. To measure flow, the amount of time for 20 drops (1 mL) of water to flow through the vessel was recorded. Each combination of pressure was repeated in triplicate, and the flow rate averaged.

Statistics

For the compression tests, R^2–statistics data were calculated to characterize the closeness of the linear fit. The close that R^2 is to 1, the greater the correlation of the collected data in a linear fashion. This is crucial in determining an accurate compressive modulus.

For the flow tests, the recorded datasets were also converted to percent changes in order to best compare differences between each perfusion model. Paired t-tests were applied between datasets of the various stiffness models for significance set at p-value < 0.01.

III. Results

Compressive Modulus

The three industrial TC-5005 phantom models tested were found to have compressive moduli of 415 ± 16 kPa, 161 ± 26 kPa, and 63 ± 4 kPa. The two agarose phantom models were measured to have compressive moduli of 56.9 ± 2 kPa and 32.2 ± 2.6 kPa. All data were fit with a linear regression and had R^2-correlation that was greater than 0.95 (Fig. 5).

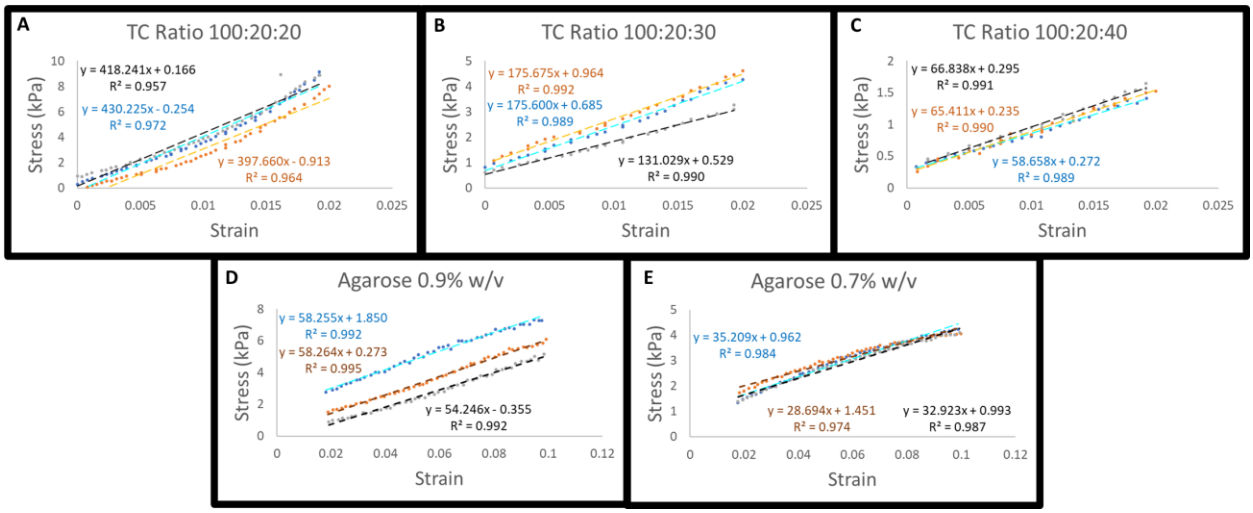

Figure 5. Compression Stress and Strain Curves of A) TC-5005 w/ 20% Agent C, B) TC-5005 w/ 30% Agent C, C) TC-5005 w/ 40% Agent C, D) 0.9% w/v Agarose, and E) 0.7% w/v Agarose

Fluid Flow

An increase in IOP in general was related to a decrease in fluid flow in our model system (Fig. 6). The fluid flow through the soft agarose phantom (E = 32 kPa) exhibited the strongest IOP related reduction with a maximum reduction of 87% in fluid flow rate (Fig. 6A, BP = 20 mmHg)

when IOP was increased from 10 to 40 mmHg. A similar trend of flow rate reduction from increased IOP was found at other tested BP levels in this phantom (Table 1).

Table 1: Percent fluid flow reduction due to IOP – in the soft scleral model (E = 32 kPa) compared to flow at IOP = 10 mmHg

BP (mmHg)	IOP (mmHg)		
	20	30	40
20	3.62	38.4	87.0
30	18.4	48.8	86.4
40	9.24	44.6	65.0

As the phantom stiffness increased, the IOP-related flow reduction showed an interesting nonlinear trend, first decreasing as the gel stiffness increased from 32 kPa to 57 kPa, and then 63 kPa. The maximum flow rate reduction in the 57 kPa model was only 39% (Fig. 6B, BP = 30 mmHg) when IOP was increased from 10 to 40 mmHg. Similarly, the flow rate reduction percentage continued to decrease in the 63 kPa model, with maximum reduction of 14% (Fig. 6A, BP = 20 mmHg) when IOP was increased from 10 to 40 mmHg. Unexpectedly, further increases in stiffness to 161 kPa and 415 kPa resulted in a reversed trend in IOP effects: that is, the maximum flow rate reduction became higher than that of 63 kPa, reaching 45% and 38%, respectively (Fig 6D and E).

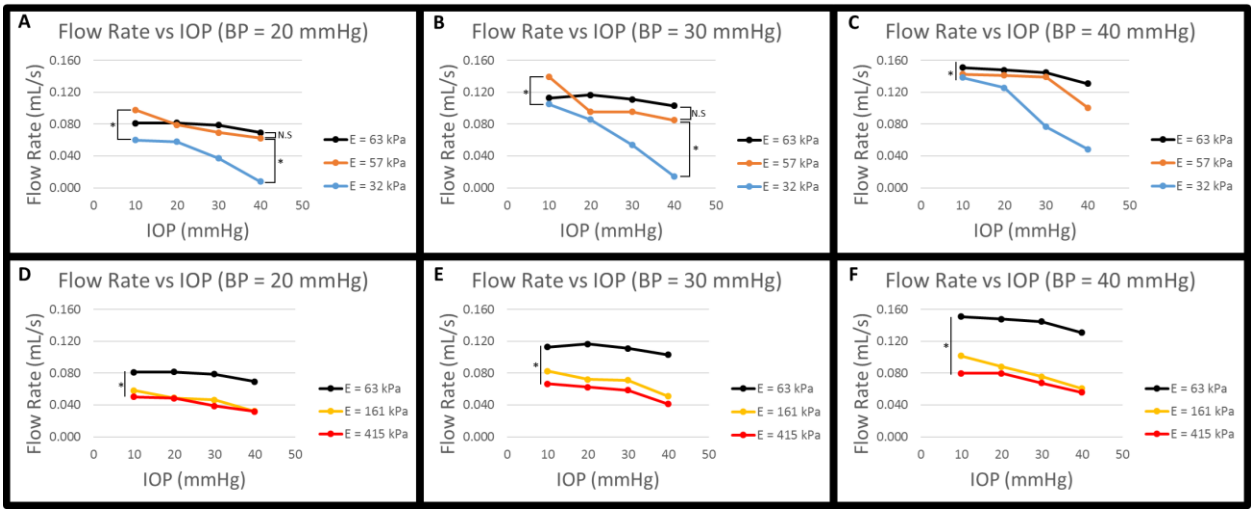

Figure 6. Fluid flow rate vs IOP at different BP intervals; (top) comparison between soft models, (bottom) comparison between stiff models

Paired t-tests were completed between different scleral models at each set BP to determine whether there was significance difference between the flow rates measured under a variable IOP. All collected datasets were found to have significant p-values less than 0.01 expect for the two models with stiffness of 57 kPa and 63 kPa with p-values of 0.25 or greater (Fig. 6).

The flow reduction for a BP of 40 mmHg at IOP from 10 to 40 mmHg are summarized in Figure 7 and Table 2.

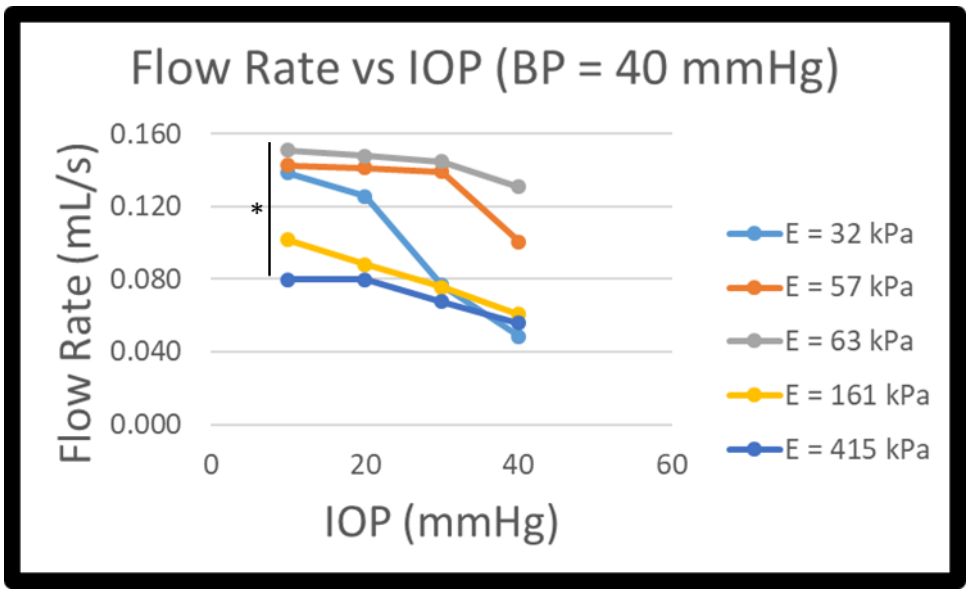

Figure 7. Fluid flow rate vs IOP at BP = 40 mmHg

Table 2: Percent fluid flow reduction due to model stiffness – at BP = 40 mmHg compared to flow at IOP = 10 mmHg

Stiffness (kPa)	IOP (mmHg)		
	20	30	40
32	9.24	44.6	65.0
56	1.13	2.62	29.6
63	2.17	4.24	13.2
161	13.3	25.4	40.2
415	-0.02	15.2	30.1

The general trend of fluid flow shows an initial increase of flow rate from the soft scleral model (E = 32 kPa) to the maximum flow rate output found in the model with stiffness of 63 kPa. A dramatic decrease in flow rate can be seen in all cases of IOP and BP combination as fluid flow decreases following subsequent increase in model stiffness (Fig. 8).

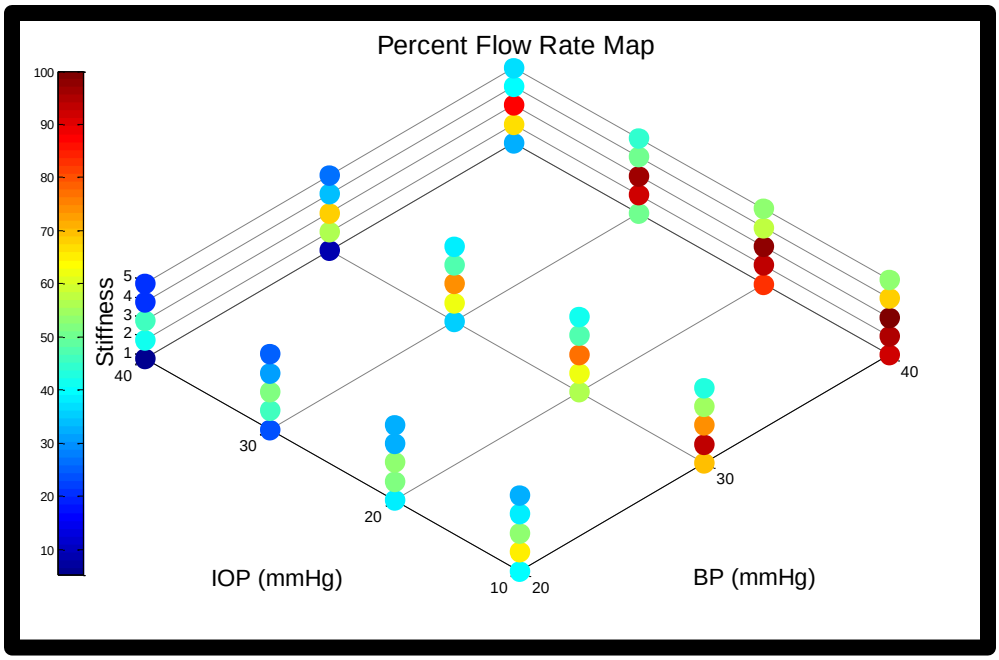

Figure 8. Percentage change in flow in response to stiffness, IOP, and BP. Stiffness: (1) = 32 kPa, (2) = 57 kPa, (3) = 63 kPa, (4) = 161 kPa, (5) = 415 kPa

Examining the slope of the flow rate reduction between IOP intervals (Fig. 6), it was observed that flow rate reduction slope was higher when IOP was greater than 20 mmHg. This trend was most noticeable in the soft scleral model (Fig. 9, Table 3) but is also present in the other models as well.

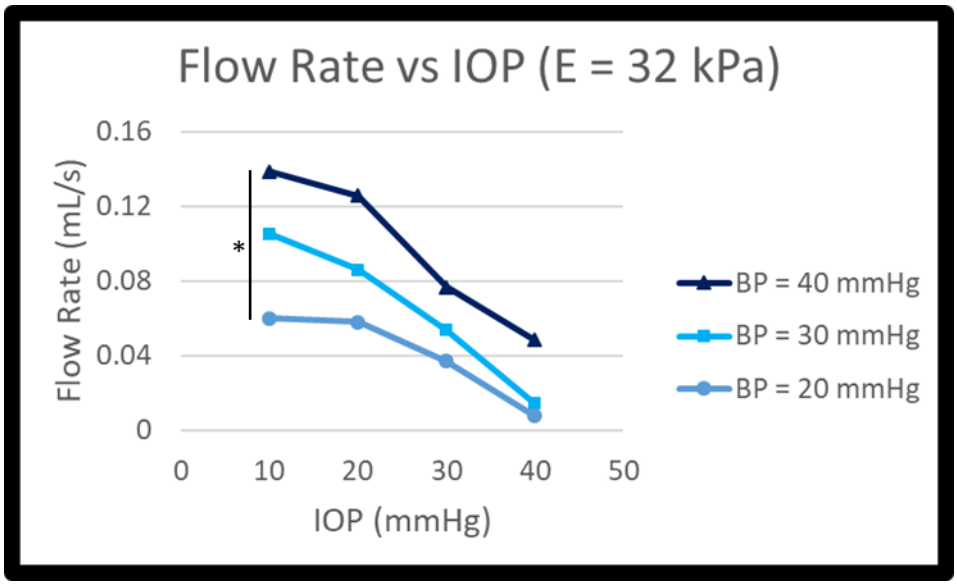

Figure 9. Fluid flow rate vs IOP in soft scleral model (E = 32 kPa)

Table 3. Flow rate reduction slope in soft scleral model (E = 32 kPa)

Reduction Slope ($\times 10^{-3}$)			
BP (mmHg)	IOP (mmHg)		
	10 to 20	20 to 30	30 to 40
20	-0.2	-2.1	-2.9
30	-1.9	-3.2	-4.0
40	-1.3	-4.9	-2.8

Change in fluid flow rate in response to changes in BP is observed more closely in Fig. 10. In all cases, increasing the BP resulted in an increase in flow rate. It is worth noting that in almost all cases, flow rate shows an almost linear increase with increasing BP. In the case of the soft scleral model (E = 32 kPa), the relationship is very clearly non-linear. Consulting Poiseuille's Law, this may be an indication of a variable resistance of the wall-less vessel.

Similar to Table 1, flow reduction due to decreasing BP are recorded in comparison to the maximum flow rate at the set IOP interval in Table 4. Using the softest phantom, for example,

decreasing BP from 40 mmHg to 30 mmHg and 20 mmHg when IOP was set at 40 mmHg reduced fluid flow by as much as 70.5% and 83.9%, respectively.

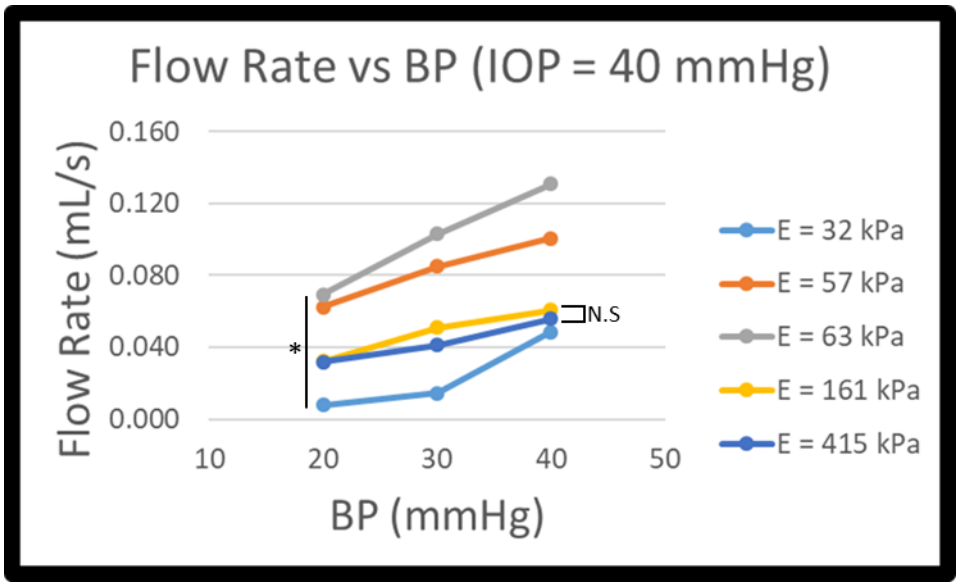

Figure 10. Fluid flow rate vs BP at IOP = 40 mmHg

Table 4. Percent fluid flow reduction due to BP – in the soft scleral model (E = 32 kPa) compared to flow at BP = 40 mmHg

BP (mmHg)	IOP (mmHg)			
	10	20	30	40
20	56.6	53.9	51.7	83.9
30	24.0	31.7	29.8	70.5

IV. Discussion/Conclusion

The pressure intervals used for IOP were selected to mimic normal IOP (10 – 20 mmHg) and ocular hypertension (> 20 mmHg). We found that elevated IOP (30 mmHg and 40 mmHg) resulted in as high as 87.0% reduction in fluid flow through the vessel when BP is at 40 mmHg.

Normal levels of IOP were found to have up to 13% reduction in flow. The exact repercussions of the flow reduction are unknown, but we hypothesize that elevated IOP may contribute to retinal ganglion cell damage through a greater lack of perfusion in comparison with normal IOP levels.

Our results in the phantom models indicated that IOP may have a significant impact on the blood flow in the arteries traversing the peripapillary sclera. For phantoms with a compressive modulus lower than 63 kPa, the flow rate reduced as IOP increased from 10 to 40 mmHg, with a higher slope of reduction when IOP was above 20 mmHg, the typical threshold of ocular hypertension. As previously reported by Ethier & Sigal, soft sclera cannot protect the ONH structures from mechanical strains during IOP elevation, which may lead to mechanical damage to the retinal ganglion cell axons passing through the scleral canal. Here, we provide evidence that soft scleral tissue may also be related to reduced blood flow to the optic nerve head during IOP elevation. This may also result in ischemic damages to the ONH and eventual axonal loss. We also observed that as scleral stiffens up to 63 KPa, there was a significantly decreased IOP-effect, providing some evidence that scleral stiffening may be protective. However, further stiffening of the sclera past 63 kPa resulted in increased IOP-effect, and thus suggesting the existence of an "optimal" scleral compressive stiffness. It is unclear what is underlying such trends.

Since BP was measured from the outflow nozzle, the pressure intervals used for BP were selected to be closer to the pressure fitting the range of a capillary network. As seen in Figure 1, the region of interest consists of the portion of the sPCA adjacent to the point of capillary branching. Appropriately, the BP range covered normal arteriole pressures (40 mmHg) down to near capillary pressures (20 mmHg). The basic model was able to show that within that range of BP, there is still a wide variation in fluid flow. Simply decreasing BP from 40 mmHg to 20 mmHg resulted in as much as 56.6% reduction in flow under normal IOP conditions. Under ocular hypertension, as

much as 83.9% reduction in fluid flow was observed in the soft scleral model. This compounded reduction in fluid flow may relate to the drastic reduction in OPP in the case that both elevated IOP and decreased BP are present. Again, the severity of the resultant reduction of fluid flow due to decreasing BP or OPP cannot be characterized through this experiment.

As described by Poiseuille's Law (see Introduction), pressure is directed related to flow rate, Q, by a resistance coefficient. In this experiment, fluid viscosity remains constant, as water is a Newtonian fluid, and the length of the vessel does not vary between experiments. This leaves the radius of the wall-less tube a potential cause for changes in resistance. Possibly, the reduction in flow occurring at higher stiffness may be a result of the resistance of the vessel against expansion that would have been caused by BP forces. At low stiffness, the vessel diameter would be variably affected by both BP and IOP in which IOP provides a compressive force while BP provides a counteracting expansive force. Increasing the stiffness of the sclera would first reduce IOP-effects, allowing BP to dominate, but then eventually also removing BP-effects when stiffening progresses beyond a certain point. The trend observed here may be an indication of how progressive stiffness may in fact provide both a protective as well as a detrimental effect to the health of the ONH from a blood flow perspective.

There are several limitations in this study. The compression tests demonstrated that agarose and, to a limited degree, industrial TC-5005 silicon are good candidates to model the mechanical stiffness of scleral tissue. The range of the compressive modulus may not have reached the reported minimum of scleral stiffness, but further experiments may be able to further reduce the stiffness of these polymers. Compression of the polymers were limited by the load cell's force capacity, and therefore may not be an accurate representation of the compressive modulus of the models at higher strain. Without measuring the exact strain resulted from IOP-simulations in the flow tests,

an exact comparison cannot be made. It can be expected that at least agarose exhibits viscoelastic properties due to its high water content. Due to this, increasing strain past a certain point will likely result in a much greater increase in stress response, resulting in an exponentially higher compressive modulus.

The perfusion model had many limitations to its design. Most importantly, sclera thickness has been experimentally determined to be approximately 1 mm to as thin as 0.8 mm due to aging (Coudrillier et al. 2012). Furthermore, the ciliary arteries are even smaller, diameter measuring to be less than 0.5 mm (Erdogmus & Govsa, 2006). The thickness of the scleral phantom in the model was measured to be approximately 20 mm with vessel diameter being at least 0.8 mm. Not only were the dimensions not biologically appropriate, mechanical limitations also prevented correct scaling of the dimensions. Moreover, the fluid flow experiments were done with water, which is not a strong substitute for blood due to its Newtonian properties. Most notably, blood is much more viscous than water, a property that contributes to fluid flow resistance that is characteristic in biology. Further work can explore models with more biologically relevant vessel and scleral dimensions as well as fluid viscosity using the same protocol.

Bibliography

Battaglioli, J. L., & Kamm, R. D. (1984). Measurements of the compressive properties of scleral tissue. *Investigative Ophthalmology & Visual Science, 25*(1), 59. Retrieved from http://www.ncbi.nlm.nih.gov/pubmed/6698732

Cherecheanu, A. P., Garhofer, G., Schmidl, D., Werkmeister, R., & Schmetterer, L. (2012). Ocular perfusion pressure and ocular blood flow in glaucoma. *Current Opinion in Pharmacology, 13*(1), 36-42. 10.1016/j.coph.2012.09.003 Retrieved from https://www.clinicalkey.es/playcontent/1-s2.0-S1471489212001609

Coudrillier, B., Campbell, I. C., Read, A. T., Geraldes, D. M., Vo, N. T., Feola, A., . . . Ethier, C. R. (2016). Effects of peripapillary scleral stiffening on the deformation of the lamina cribrosa. *Investigative Ophthalmology & Visual Science, 57*(6), 2666. 10.1167/iovs.15-18193 Retrieved from http://www.ncbi.nlm.nih.gov/pubmed/27183053

Coudrillier, B., Tian, J., Alexander, S., Myers, K. M., Quigley, H. A., & Nguyen, T. D. (2012). Biomechanics of the human posterior sclera: Age- and glaucoma-related changes measured using inflation testing. Investigative Ophthalmology & Visual Science, 53(4), 1714. 10.1167/iovs.11-8009 Retrieved from http://www.ncbi.nlm.nih.gov/pubmed/22395883

Diekmann, H., & Fischer, D. (2013a). Glaucoma and optic nerve repair. *Cell and Tissue Research, 353*(2), 327-337. 10.1007/s00441-013-1596-8 Retrieved from http://www.ncbi.nlm.nih.gov/pubmed/23512141

Fazio, M., Grytz, R., Morris, J., Bruno, L., Gardiner, S., Girkin, C., & Downs, J. (2014). Age-related changes in human peripapillary scleral strain. *Biomechanics and Modeling in Mechanobiology, 13*(3), 551-563. 10.1007/s10237-013-0517-9 Retrieved from http://www.ncbi.nlm.nih.gov/pubmed/23896936

Hayreh, S. S., & Edwards, J. (1971). Ophthalmic arterial and venous pressures. Brit. J. Ophthal., 55, 649-663. Retrieved from doi: 10.1136/bjo.55.10.649

Hamzah, J. C., & Azuara-Blanco, A. (2010). What is the best method for diagnosing glaucoma? *Expert Review of Ophthalmology, 5*(4), 463+. Retrieved from http://dx.doi.org/10.1586/eop.10.33

He, Z., Vingrys, A. J., Armitage, J. A., & Bui, B. V. (2011). The role of blood pressure in glaucoma. *Clinical and Experimental Optometry, 94*(2), 133-149. 10.1111/j.1444-0938.2010.00564.x Retrieved from http://onlinelibrary.wiley.com/doi/10.1111/j.1444-0938.2010.00564.x/abstract

Jia, X., Yu, J., Liao, S., & Duan, X. (2016). Biomechanics of the sclera and effects on intraocular pressure. *International Journal of Ophthalmology, 9*(12), 1824-1831. Retrieved from http://lib.cqvip.com/qk/60944X/201612/670831428.html

Johnston, P. R., Johnston, B. M., Corney, S., & Kilpatrick, D. (2004). Non-newtonian blood flow in human right coronary arteries: Steady state simulations. Journal of Biomechanics, 37(5), 709-720. 10.1016/j.jbiomech.2003.09.016 Retrieved from https://www.sciencedirect.com/science/article/pii/S0021929003003579

Kiel, J. W., Hollingsworth, M., Rao, R., Chen, M., & Reitsamer, H. A. (2011). Ciliary blood flow and aqueous humor production.*Progress in Retinal and Eye Research, 30*(1), 1-17. 10.1016/j.preteyeres.2010.08.001 Retrieved from https://www.sciencedirect.com/science/article/pii/S1350946210000546

Klein, B. E. K., Klein, R., & Knudtson, M. D. (2005). Intraocular pressure and systemic blood pressure: Longitudinal perspective: The beaver dam eye study. *The British Journal of*

Ophthalmology, 89(3), 284-287. 10.1136/bjo.2004.048710 Retrieved from http://www.ncbi.nlm.nih.gov/pubmed/15722304

Lombard, W. P. (1912). The blood pressure in the arterioles, capillaries, and small veins of the human skin. American Physiological Society,

Mortazavi, A. M., Simon, B. R., Stamer, W. D., & Vande Geest, J. P. (2009). Drained secant modulus for human and porcine peripapillary sclera using unconfined compression testing. *Experimental Eye Research, 89*(6), 892-897. 10.1016/j.exer.2009.07.011 Retrieved from https://www.sciencedirect.com/science/article/pii/S0014483509002218

Palko, J. R., Morris, H. J., Pan, X., Harm, C. D., Koehl, K. L., Gelatt, K. N., . . . Liu, J. (2016). Influence of age on ocular biomechanical properties in a canine glaucoma model with ADAMTS10 mutation. *PLoS ONE, 11*(6), 1-19. Retrieved from https://doi.org/10.1371/journal.pone.0156466

Pillunat, L. E., Anderson, D. R., Knighton, R. W., Joos, K. M., & Feuer, W. J. (1997). Autoregulation of human optic nerve head circulation in response to increased intraocular pressure. *Experimental Eye Research, 64*(5), 737-744. 10.1006/exer.1996.0263 Retrieved from https://www.sciencedirect.com/science/article/pii/S0014483596902638

Prada, D., PhD, Harris, Alon, MS, PhD, FARVO, Guidoboni, G., PhD, Siesky, B., PhD, Huang, A. M., BS, & Arciero, J., PhD. (2016). Autoregulation and neurovascular coupling in the optic nerve head. *Survey of Ophthalmology, 61*(2), 164-186. 10.1016/j.survophthal.2015.10.004 Retrieved from https://www.clinicalkey.es/playcontent/1-s2.0-S0039625715001824

Qin, S., Caskey, C. F., & Ferrara, K. W. (2009). Ultrasound contrast microbubbles in imaging and therapy: Physical principles and engineering. *Physics in Medicine and Biology, 54*(6),

R57. 10.1088/0031-9155/54/6/R01 Retrieved from http://iopscience.iop.org/0031-9155/54/6/R01

Quigley, H., & Cone, F. (2013). Development of diagnostic and treatment strategies for glaucoma through understanding and modification of scleral and lamina cribrosa connective tissue. *Cell and Tissue Research, 353*(2), 231-244. 10.1007/s00441-013-1603-0 Retrieved from http://www.ncbi.nlm.nih.gov/pubmed/23535950

Ramanathan, S., & Ernest, J. T. (1998). What is glaucoma? *Perspectives in Biology and Medicine, 42*(1), 8-13. 10.1353/pbm.1998.0028 Retrieved from https://muse.jhu.edu/article/401392

Rickey, D. W., Picot, P. A., Christopher, D. A., & Fenster, A. (1995). A wall-less vessel phantom for doppler ultrasound studies.*Ultrasound in Medicine & Biology, 21*(9), 1163-1176. 10.1016/0301-5629(95)00044-5 Retrieved from https://www.sciencedirect.com/science/article/pii/0301562995000445

Riva, C. E., Cranstoun, S. D., & Petrig, B. L. (1996). Effect of decreased ocular perfusion pressure on blood flow and the flicker-induced flow response in the cat optic nerve head. *Microvascular Research, 52*(3), 258-269. 10.1006/mvre.1996.0063 Retrieved from https://www.sciencedirect.com/science/article/pii/S0026286296900631

Schmidl, D., Garhofer, G., & Schmetterer, L. (2011). The complex interaction between ocular perfusion pressure and ocular blood flow – relevance for glaucoma. *Experimental Eye Research, 93*(2), 141-155. 10.1016/j.exer.2010.09.002 Retrieved from https://www.sciencedirect.com/science/article/pii/S0014483510002976

Sigal, I. A., & Ethier, C. R. (2009). Biomechanics of the optic nerve head. *Experimental Eye Research, 88*(4), 799-807. 10.1016/j.exer.2009.02.003 Retrieved from https://www.sciencedirect.com/science/article/pii/S0014483509000359

Sutera, S. P. (1993). The history of poiseuille's law. Annu. Rev. Fluid Mech., 25, 1-20. Retrieved from www.annualreviews.org

Wensor, M. D., McCarty, C. A., Stanislavsky, Y. L., Livingston, P. M., & Taylor, H. R. (1998). The prevalence of glaucoma in the melbourne visual impairment project. *Ophthalmology, 105*(4), 733-739. 10.1016/S0161-6420(98)94031-3 Retrieved from https://www.sciencedirect.com/science/article/pii/S0161642098940313

Worthington, K. S., Wiley, L. A., Bartlett, A. M., Stone, E. M., Mullins, R. F., Salem, A. K., . . . Tucker, B. A. (2014). Mechanical properties of murine and porcine ocular tissues in compression. *Experimental Eye Research, 121*, 194-199. 10.1016/j.exer.2014.02.020 Retrieved from http://www.ncbi.nlm.nih.gov/pubmed/24613781